



Cite this: *CrystEngComm*, 2023, **25**, 1067

## A series of cation-modified robust zirconium-based metal-organic frameworks for carbon dioxide capture†

Guoyu Zhang,<sup>a</sup> Feng Xie,<sup>a</sup> Thomas M. Osborn Popp,<sup>a</sup> Akash Patel,<sup>a</sup> Eder Moisés Cedeño Morales,<sup>b</sup> Kui Tan,<sup>b</sup> Ryan Crichton,<sup>a</sup> Gene Hall,<sup>a</sup> Jianyuan Zhang,  <sup>a</sup> Andrew J. Nieuwkoop<sup>a</sup> and Jing Li  <sup>\*a</sup>

Metal-organic frameworks (MOFs) represent one of the most promising porous solids for possible use as sorbents to control and reduce the greenhouse gas emission. Studies have shown that open metal sites (OMS) interact strongly with carbon dioxide and thus, serve as efficient binding sites for CO<sub>2</sub> capture. However, many OMS-bearing MOFs are lack of framework stability and often have high regeneration temperature. To seek ways to solve the stability issue, we designed a series of isoreticular MOFs, Zr-tcpb-COOM (M = alkali/alkaline earth metal), by exchange of protons with metal ions on Zr-tcpb-COOH via post-synthetic modification (PSM). The pristine MOF (Zr-tcpb-COOH) has a very robust framework. The PSM process does not deteriorate the framework stability but creates metal binding sites that form strong bonds with carbon dioxide. The results show that at low CO<sub>2</sub> pressure, the uptake amount is enhanced considerably using Zr-tcpb-COOM and is in trend of increasing atomic number (Li<sup>+</sup> < Na<sup>+</sup> < K<sup>+</sup> < Ca<sup>2+</sup>). High adsorption selectivity (CO<sub>2</sub>/N<sub>2</sub> IAST selectivity (15 : 85) = 539.5) is also achieved for CO<sub>2</sub> over N<sub>2</sub> at room temperature. This approach offers a feasible method to improve CO<sub>2</sub> capture capacity, especially at low concentrations.

Received 7th December 2022,  
Accepted 5th January 2023

DOI: 10.1039/d2ce01633h

rsc.li/crystengcomm

### 1. Introduction

Due to the booming industrialization and population increase in the last century, the emission of greenhouse gases has become an inevitable problem.<sup>1,2</sup> Climate change, largely induced by the rapid increase of such emissions, is a major challenge of our era.<sup>3</sup> History will look back at this period and reflect on what contributions scientists have made. Besides relying on developing renewable clean energy and improving the energy efficiency of current technologies, negative emissions technologies (NETs) are the answer to this historical strait.<sup>4,5</sup> Traditional NET mainly utilizes amine/inorganic based aqueous solutions to adsorb CO<sub>2</sub> and dispose carbamate or bicarbonate forms of CO<sub>2</sub> from the solution phase. However, this technology faces several drawbacks such as significant energy input for regeneration due to large heat capacity, bulky volume occupancy, high corrosion, and degradation.<sup>6,7</sup> Its replacement by more advanced technologies is urgently demanded globally.

Adsorption based technologies using highly porous solids have been considered as the next generation of NETs because of the large capacity, high selectivity, and relatively low regeneration energy associated with these technologies.<sup>8</sup> Metal-organic frameworks (MOFs) are one of the most promising candidates among the known sorbents, not only because they have all the desired features mentioned above, but also because they possess unbeatable tunability and functionality.<sup>9–13</sup> Although high adsorption capacity for CO<sub>2</sub> has been achieved by MOFs, many of them only perform well at higher pressure/concentration; others that do take up sufficiently high amount of CO<sub>2</sub> at low concentrations (*e.g.*, in ambient air, ~400 ppm) are usually *via* chemisorption. The easy functionalization of MOFs allows creation of strong CO<sub>2</sub>-MOF interaction sites to selectively capture CO<sub>2</sub> over other abundant gases such as N<sub>2</sub>, O<sub>2</sub>, CH<sub>4</sub>, *etc.*<sup>1,10</sup> Thus far, MOFs with four types of binding sites have been largely used for the selective chemisorption of CO<sub>2</sub>: 1) amine-appended sites;<sup>14–18</sup> 2) M-OH active sites (M = Zn, Co, Ni, Mn);<sup>19–21</sup> 3) NH<sub>2</sub> functionalized sites of ligands;<sup>22–24</sup> and 4) OMS,<sup>25–29</sup> all of which have shown good performance regarding capacity and selectivity. However, MOFs in the first two groups suffer consistently from the loss of active sites after long-term usage and thus, have low recyclability.<sup>7,30</sup> The third method requires extra steps in ligand synthesis and sometimes suffers from amine oxidation, resulting in high cost.

<sup>a</sup> Department of Chemistry and Chemical Biology, Rutgers University, 123 Bevier Road, Piscataway, New Jersey 08854, USA. E-mail: jingli@rutgers.edu

<sup>b</sup> Department of Materials Science and Engineering, University of Texas at Dallas, 800 West Campbell Road, Richardson, Texas, 75080, USA

† Electronic supplementary information (ESI) available: PXRD, XPS, NMR, XRF, *etc.* See DOI: <https://doi.org/10.1039/d2ce01633h>

Comparably, the creation of OMS (the fourth method) is a straightforward and effective way to boost  $\text{CO}_2$  affinity and enhance the uptake amount significantly at low concentrations. However, often MOFs with OMS are water/moisture sensitive and can't be sustained under ambient conditions for long period of time. In addition, if generation of OMS must be done by heating (in cases where solvent exchange are unsuccessful) the temperature required to remove the coordinated solvents with high boiling points (e.g., DMF & DMA) will be rather high, which may cause structure collapse.<sup>31,32</sup> To address these issues, we have attempted to embed reactive metal sites into a robust MOF that does not have OMS *via* post-synthetic modification (PSM) process. This approach also allows us to introduce different metal ions into the same structure by the same method to tune the  $\text{CO}_2$  capture performance. Only a few papers using similar approach have been reported<sup>33–35</sup> for  $\text{CO}_2$  capture and none of them have carried out a systematic study to compare the performance of different metal cations.

Herein, we report the synthesis of a 4,8-connected zirconium-based metal-organic framework Zr-tcpb-COOH made of a hexacarboxylate ligand (1,2,4,5-tetrakis(4-carboxyphenyl)-3,6-dicarboxyl-benzene,  $\text{H}_4\text{tcpb-(COOH)}_2$ ) and its cation exchanged form, Zr-tcpb-COOM (M = Li, Na, K, and Ca) by PSM process. The original structure Zr-tcpb-COOH, which contains two free, non-coordinated carboxylic groups, is isoreticular to Zr-tcpb (CAU-24).<sup>36</sup> The unbonded carboxylic acid groups in Zr-tcpb-COOH can react readily with  $\text{M}^+/\text{M}^{2+}$  in basic alkali/alkaline solutions through acid-base neutralization to form Zr-tcpb-COOM, which are then used to evaluate the  $\text{CO}_2$  adsorption performance. The results reveal that at the low concentration of  $\text{CO}_2$ , the uptake amounts of these metal cation embedded Zr-tcpb-COOM MOFs show obvious enhancement, and the uptake capacity increases as a function of increasing atom number of the metal cations ( $\text{Li}^+ < \text{Na}^+ < \text{K}^+ < \text{Ca}^{2+}$ ). Furthermore, the Zr-tcpb-COOM MOFs exhibit high moisture and chemical stability, thermal stability, and recyclability.

## 2. Experimental section

### 2.1 General information

All reagents were used as purchased unless specified otherwise. Detailed information about the sources of chemicals is provided in the ESI.†

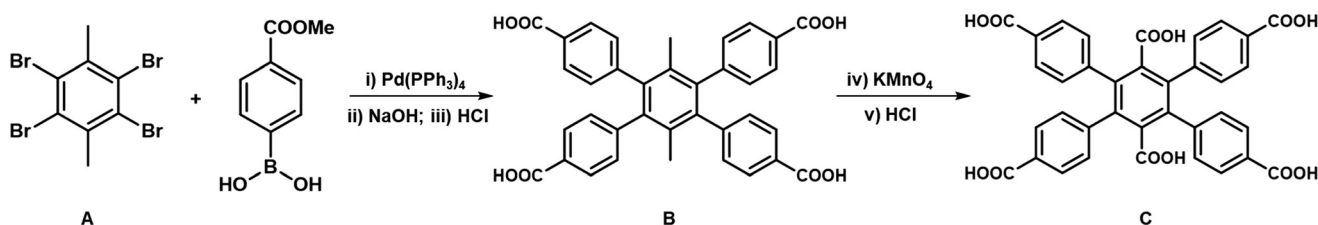
### 2.2 Synthesis of ligand $\text{H}_4\text{tcpb-(COOH)}_2$

The hexacarboxylic acid 1,2,4,5-tetrakis(4-carboxyphenyl)-3,6-dicarboxyl-benzene ( $\text{H}_4\text{tcpb-(COOH)}_2$ ) was synthesized through the Suzuki Coupling reactions and subsequent oxidation (Scheme 1). In a 500 mL three-necked round bottom flask, 1,2,4,5-tetrabromo-3,6-dimethyl-benzene (A) (2.1 g, 5 mmol), 4-methoxycarbonylphenylboronic acid (5.4 g, 30 mmol),  $\text{K}_3\text{PO}_4$  (6.36 g, 30 mmol), and  $\text{Pd}(\text{PPh}_3)_4$  (0.578 g, 0.5 mmol) were mixed in degassed 1,4-dioxane (200 mL). The mixture was heated at 90 °C under nitrogen atmosphere for 3 days. The reaction was monitored by TLC. After the starting materials disappeared, the organic solvent was then removed under reduced pressure and 120 mL of water was added to the solid residual which was extracted by dichloromethane (3 × 60 mL). The organic phases were combined, washed with brine, and dried over  $\text{MgSO}_4$  overnight. The organic solvent was removed by rotary evaporation to give the crude product which was purified by column chromatography (eluent: hexane/ethyl acetate = 4:1). The obtained ester was then hydrolyzed in a mixture of NaOH aqueous solution (6 M, 50 mL), tetrahydrofuran (50 mL), and methanol (50 mL) by reflux overnight to give the pure form of compound B, 1,2,4,5-tetrakis(4-carboxyphenyl)-3,6-dimethyl-benzene ( $\text{H}_4\text{-tcpb-(Me)}_2$ ) (2.1 g, yield: 73%).  $^1\text{H}$  NMR (500 MHz, DMSO-d6,  $\delta$ ): 1.64 (s, 6H,  $\text{CH}_3$ ), 7.19 (d, 8H, Ar H), 7.72 (d, 8H, Ar H), 12.87 (s, 4H, COOH).

In a 250 mL round bottom flask, compound B (2 g, 3.4 mmol) was dissolved in a mixture of NaOH aqueous solution (2 M, 100 mL) and *t*BuOH (30 mL). Then, 6 g of  $\text{KMnO}_4$  was slowly added to the solution over 3 days (2 g each day) at 80 °C. After the color of the  $\text{KMnO}_4$  solution faded, the clear filtrate was obtained *via* reducing pressure filtration. The final product of compound C could be precipitated out by acidifying the solution with 6 M HCl aqueous solution and was further dried in the vacuum oven at 80 °C overnight (1.8 g, yield: 89%).  $^1\text{H}$  NMR (500 MHz, DMSO-d6,  $\delta$ ): 7.26 (d, 8H, Ar H), 7.70 (d, 8H, Ar H), 12.91 (s, 6H, COOH). Peaks of compound B and C are assigned and integrated to confirm the structures (Fig. S1 and S2†).

### 2.3 Synthesis of Zr-tcpb, Zr-tcpb-Me and Zr-tcpb-COOH

**Synthesis of Zr-tcpb.** Zr-tcpb was synthesized *via* a solvothermal reaction according to the previous procedure (CAU-24).<sup>36</sup>  $\text{ZrOCl}_2 \cdot 8\text{H}_2\text{O}$  (85 mg, 0.26 mmol) and  $\text{H}_4\text{tcpb}$  (29.8 mg, 0.05 mmol) was dispersed in a mixture of DMF (3



Scheme 1 Synthesis of 1,2,4,5-tetrakis(4-carboxyphenyl)-3,6-dicarboxyl-benzene ( $\text{H}_4\text{tcpb-(COOH)}_2$ ).

mL) and formic acid (1 mL) solution in a 20 mL glass vial. The mixture was then sonicated for 30 minutes. The vial was capped tightly and put into a pre-heated 120 °C oven overnight. The white crystalline precipitate was filtrated and washed with fresh DMF and MeOH several times. The product was characterized by PXRD.

**Synthesis of Zr-tcpb-Me.** Zr-tcpb-Me was synthesized *via* a solvothermal reaction.  $\text{ZrOCl}_2 \cdot 8\text{H}_2\text{O}$  (85 mg, 0.26 mmol) and  $\text{H}_4\text{tcpb-(Me)}_2$  (31.23 mg, 0.05 mmol) was added to a mixture of DMF (3 mL) and formic acid (1.5 mL) solution in a 20 mL glass vial. The mixture was then sonicated for 30 minutes. The vial was capped tightly and put into a pre-heated 120 °C oven overnight. The white precipitate was obtained after filtration and washing with fresh DMF and MeOH several times. The product was characterized by PXRD.

**Synthesis of Zr-tcpb-COOH.** Zr-tcpb-COOH was synthesized *via* a solvothermal reaction.  $\text{ZrOCl}_2 \cdot 8\text{H}_2\text{O}$  (42.5 mg, 0.13 mmol) and  $\text{H}_4\text{tcpb-(COOH)}_2$  (17.3 mg, 0.025 mmol) was added to a mixture of DMA (4 mL) and formic acid (2 mL) solution in a 20 mL glass vial. The mixture was then sonicated for 30 minutes. The vial was capped tightly and put into a pre-heated 120 °C oven for 3 days. The white precipitate was obtained after filtration and washing with fresh DMA and MeOH several times. The product was characterized by PXRD.

#### 2.4 Post-synthetic modification of Zr-tcpb-COOH

As-made Zr-tcpb-COOH samples (100 mg each) were soaked in 20 mL of fresh MeOH and kept at room temperature overnight. The sample was then filtered and immersed into corresponding 0.01 M aqueous alkali/alkaline solutions (LiOH, NaOH, KOH, and  $\text{Ca}(\text{OH})_2$ ) and stirred at 40 °C overnight. The base-treated samples were filtered and washed with  $3 \times 10$  mL of DI water and  $2 \times 10$  mL of MeOH. The presence of alkali/alkaline cation was analyzed and confirmed by solid-state NMR (ss-NMR), X-ray fluorescence (XRF) and X-ray photoelectron spectroscopy (XPS) measurement.

#### 2.5 Gas adsorption measurements

Gas adsorption measurements were carried out on a Micromeritics 3Flex volumetric adsorption analyzer. Liquid nitrogen and a circulating-bath with digital temperature controller were used for measurements at 77 K and temperatures near room temperature, respectively. For each adsorption measurement, around 80 mg as-synthesized sample was used and activated at 100 °C under dynamic vacuum for 6 hours prior to adsorption experiments.

The single-component isotherms for  $\text{CO}_2$  recyclability experiment and  $\text{H}_2\text{O}$  adsorption were collected in a gravimetric adsorption analyzer TGA Q50 (TA Instruments). For water adsorption experiments, pure  $\text{N}_2$  gas was purged through the bubbler containing water and was performed as the carrier gas of saturated water vapor. The partial pressure of  $\text{CO}_2$  or  $\text{H}_2\text{O}$  was adjusted by controlling the ratio of pure  $\text{N}_2$  gas and  $\text{CO}_2$  or saturated water vapor. Approximately 20 mg of samples was

activated under a constant  $\text{N}_2$  flow for 30 min at 373 K. Adsorbed amounts were monitored by weight changes in the sample and continuously monitored throughout the experiments.

#### 2.6 Solid-state NMR experiments

Solid state NMR spectra were acquired at 9.4 T using a Bruker Avance III spectrometer equipped with a Bruker 3.2 mm HXY probe, using a frequency of 400.2 MHz for  $^1\text{H}$ , 155.5 MHz for  $^7\text{Li}$ , 105.9 MHz for  $^{23}\text{Na}$ , and 100.6 MHz for  $^{13}\text{C}$ . All spectra were acquired at 20 °C and 20 kHz MAS.  $^{13}\text{C}$  cross polarization (CP) MAS experiments were acquired using a 5 ms contact period, 2 s inter-scan delay, and 100 kHz TPPM  $^1\text{H}$  decoupling during acquisition.  $^1\text{H}$ ,  $^7\text{Li}$ , and  $^{23}\text{Na}$  spectra were collected using a  $\pi/2$  pulse-acquire sequence, with inter-scan delays set to approximately  $5 \times T_1$  at 2 s, 3 s, and 0.5 s for  $^1\text{H}$ ,  $^7\text{Li}$ , and  $^{23}\text{Na}$  respectively. Chemical shifts were referenced to the downfield  $^{13}\text{C}$  resonance of adamantane at 38.48 ppm.

#### 2.7 FT-IR measurement

IR measurements were performed on a Nicolet 6700 FTIR spectrometer equipped with a liquid  $\text{N}_2$ -cooled mercury cadmium telluride MCT-A detector. The sample of MOF compound (Zr-tcpb-COOH, Zr-tcpb-COOLi, Zr-tcpb-COONa, and Zr-tcpb-COOK) (~2 mg each) was pressed onto a KBr pellet and placed into a vacuum cell placed at the focal point of the sample compartment of the infrared spectrometer. The cell was connected to a vacuum line for evacuation. All spectra were recorded under vacuum (base pressure <20 mTorr) in transmission mode with a frequency range of 600–4000  $\text{cm}^{-1}$  (4  $\text{cm}^{-1}$  spectral resolution).

### 3. Results and discussion

It is well known that one of the most stable MOF families are zirconium-based compounds built on  $\text{Zr}_6$  hexanuclear clusters (Fig. 1a) with a maximum 12-connectivity. They also feature well-controlled synthesis, easy reproducibility and rich structural tunability.<sup>37</sup> In general, it is straightforward to obtain isoreticular structures with the same topology, simply by functionalizing the parent ligands,<sup>38</sup> for example, adding small functional groups without changing their overall length and connectivity. Therefore, taking the parent structure of Zr-tcpb (CAU-24),<sup>36</sup> we functionalized ligand by adding methyl group and carboxylic group to the central benzene ring. The MOF synthesis conditions with the modified ligands were adjusted and two isoreticular MOFs Zr-tcpb-Me and Zr-tcpb-COOH were successfully synthesized under solvothermal reactions. Two free carboxylic acid groups added to the ligands were not bonded to the zirconium clusters and will thus be available as binding sites for alkali/alkaline metal ions *via* PSM procedure (Fig. 1b). The powder X-ray diffraction (PXRD) patterns of the as-made samples of Zr-tcpb-Me and Zr-tcpb-COOH match well with the as-made sample of Zr-tcpb as well as the simulated pattern

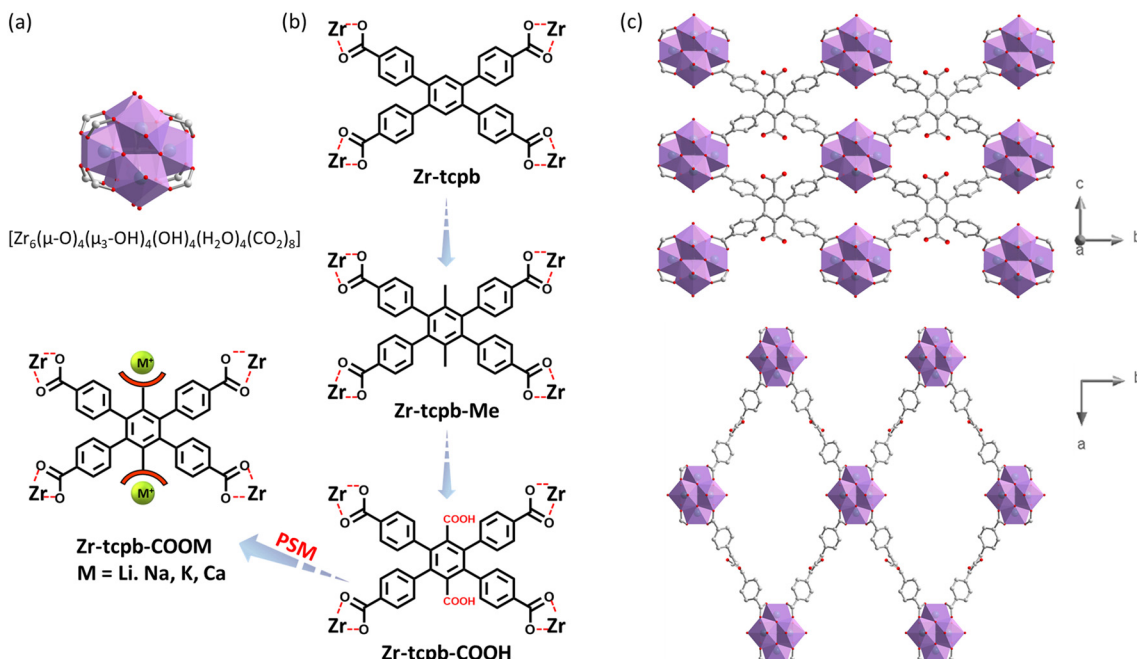


**Fig. 1** (a) The hexanuclear 8-connected  $\text{Zr}_6$  cluster; (b) The experimental design of Zr-tcpb-X series through ligand functionalization and post-synthetic modification (PSM) for  $\text{CO}_2$  capture; (c) Simulated structure of Zr-tcpb-COOH views along  $a$ -axis (top) and  $c$ -axis (bottom) which both have 1-D channels through the axis and featured a scu topology. Color code: C – grey; O – red; Zr – cyan.

(Fig. 2a), confirming that the ligand functionalized structures are isoreticular to the parent structure. We also obtained simulated structure of Zr-tcpb-COOH using crystal builder and material visualizer modules of Material Studio 7 (Fig. 1c). Like the parent structure, it crystallizes in a C-centered orthorhombic system with space group  $Cmmm$  and features a 4,8-connected scu topology. The structure contains 1D open channels along both the  $a$ -axis and  $c$ -axis. While the channels along the  $a$ -axis may be too small, those along the  $c$ -axis are more than enough to accommodate metal cations at the free  $-\text{COOH}$  sites. All three isoreticular MOFs, Zr-tcpb, Zr-tcpb-Me and Zr-tcpb-COOH exhibit high thermal stability. Thermogravimetric (TG) analysis show that their decomposition temperatures are above 400 °C (Fig. 2c).

### 3.1 Synthesis and structure characterization

### 3.2 Metal cation incorporation via post-synthetic modification

To prepare the as-made Zr-tcpb-COOH for metal site incorporation, we carried out solvent exchange by immersing the sample in fresh MeOH, which was followed by treating with 0.01 M alkaline basic solution. The PXRD patterns of the base-treated samples remained unchanged (Fig. 2b), indicating the integrity of the frameworks. Similar thermal stability was also observed for the samples after treatment (Fig. 2c). We hypothesized that the acid–base neutralization will result in strong bonds between the metal cations and free carboxylic groups. The infrared (IR) spectroscopy was employed to examine and verify this hypothesis. As shown in Fig. 2d, the IR spectrum

of Zr-tcpb-COOH is dominated by the absorption bands associated with the vibrations of the organic linker, *e.g.*, stretching modes  $\nu_{\text{as},\text{s}}$  of carboxylic group around 1600 and 1400  $\text{cm}^{-1}$ ,<sup>39</sup> in plane/out of plane deformation modes  $\delta_{\text{ip},\text{oop}}$  of phenyl ring CH at 1018 and 867  $\text{cm}^{-1}$ .<sup>40,41</sup> Our previous studies have shown that the frequency of these modes is sensitive to its chemical environment.<sup>41–43</sup> The un-bonded carboxylic group of the  $\text{H}_4\text{tcpb}-(\text{COOH})_2$  linker is characterized by its featured bands  $\nu(\text{C}=\text{O})$  at 1715  $\text{cm}^{-1}$  and  $\nu(\text{C}-\text{OH})$  at 1222  $\text{cm}^{-1}$ . After the treatment in alkali hydroxide solution, most bands remained in the same positions except for  $\nu(\text{C}-\text{OH})$  that shifted upward slightly to 1228  $\text{cm}^{-1}$ . This further indicates that alkali/alkaline ions interact primarily with the  $-\text{COOH}$  moiety of the linkers. In addition, we notice the loss of the  $\nu(\text{OH})$  band at 3670  $\text{cm}^{-1}$  that is attributed to the stretching mode of terminal and bridge  $-\text{OH}/\text{H}_2\text{O}$  on  $\text{Zr}_6\text{O}_4$  clusters,<sup>44</sup> which suggests that hydroxide also reacted with these species (Fig. S4†). The presence of the characteristic peaks in the X-ray fluorescence (XRF) spectra (Fig. S5†) and X-ray photoelectron spectroscopy (XPS) plots (Fig. S6†) offers further evidence of the success of post-synthetic modification. The loading percentage was calculated to be 0.66 K and 0.71 Ca per ligand, respectively. The small difference in the conversion amount between the K and Ca samples is likely due to the longer treatment time and repeated treatment of the latter.

### 3.3 Gas adsorption analysis

The permanent porosity of Zr-tcpb-COOM was evaluated using  $\text{N}_2$  adsorption isotherm data collected at 77 K. The solvent-exchanged materials were activated at 373 K for 6

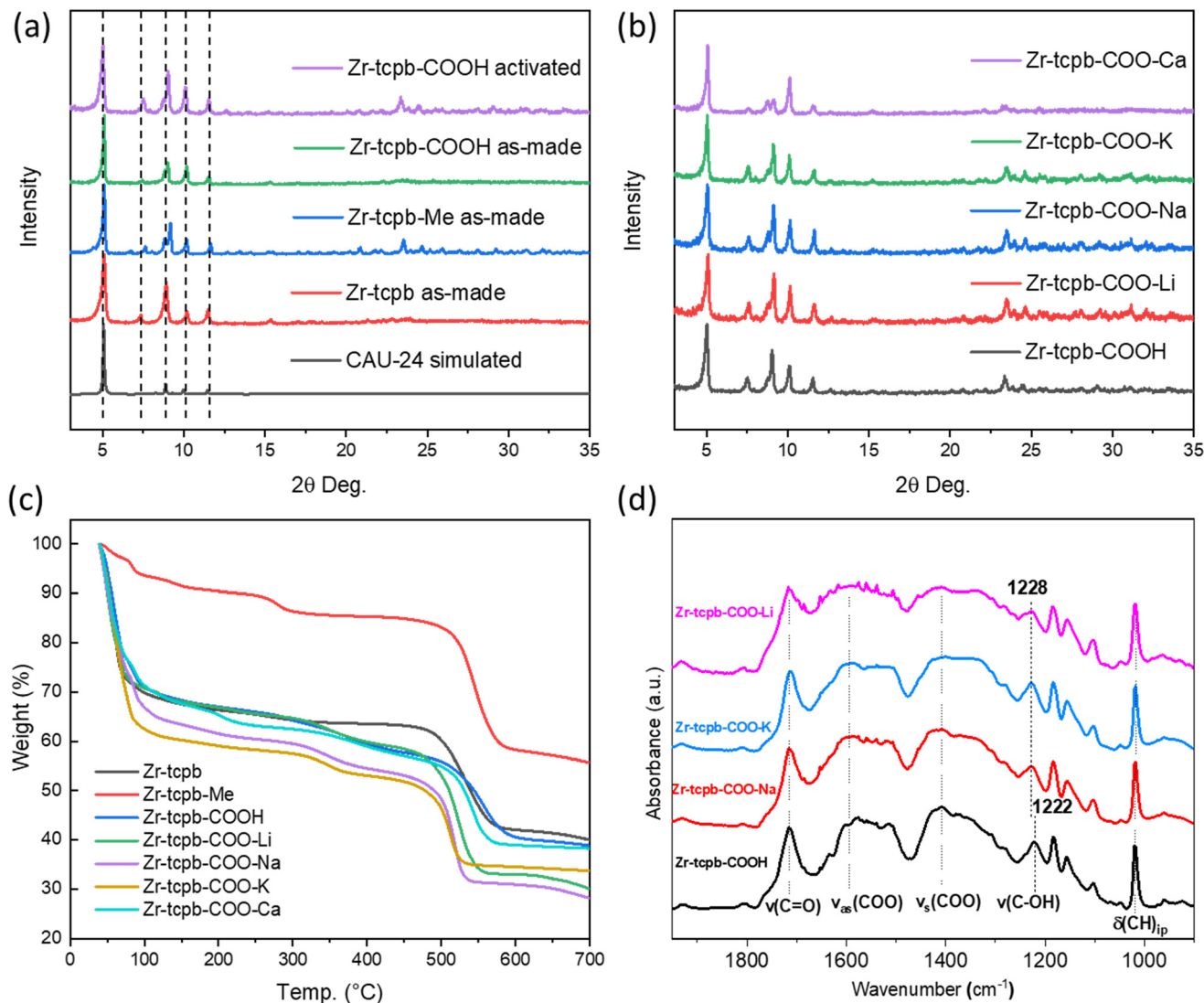


**Fig. 2** Powder X-ray diffraction patterns of isoreticular series of Zr-tcpb-X MOFs before (a) and after (b) treatment of alkali/alkaline aqueous solutions. The peaks match well with those of the simulated structure of CAU-24; (c) the thermogravimetric (TG) plots of the Zr-tcpb-X and Zr-tcpb-COO series; (d) IR spectra of Zr-tcpb-COOH and samples after treating with alkali hydroxide solutions. All spectra are referenced to the blank KBr under vacuum. Notation and acronym:  $\nu$ , stretching;  $\delta$ , deformation; ip, in plane; as, asymmetric; and s, symmetric.

hours under high vacuum to remove the solvent molecules and coordinated water in the frameworks. All the  $N_2$  isotherms show a two-step uptake indicating the presence of two types of pores (Fig. 3a). Additionally, the quantity adsorbed decreased with the increase of atomic number which is reasonable since the molecular weight of sorbents increased accordingly. The estimated Brunauer–Emmett–Teller (BET) surface area values are  $1075\text{ m}^2\text{ g}^{-1}$  (Zr-tcpb-COOH),  $837\text{ m}^2\text{ g}^{-1}$  (Zr-tcpb-COOLi),  $828\text{ m}^2\text{ g}^{-1}$  (Zr-tcpb-COONa),  $747\text{ m}^2\text{ g}^{-1}$  (Zr-tcpb-COOK), and  $632\text{ m}^2\text{ g}^{-1}$  (Zr-tcpb-COOCa), respectively. The pore size distribution was calculated by the Horvath–Kawazoe model. The original  $15\text{ \AA}$  pore along the  $c$ -axis slightly shrunk owing to the occupancy of the larger metal cations (Fig. S7†).

Single component adsorption isotherms of carbon dioxide were measured at room temperature (298 K). The samples

were activated under the same conditions as described earlier. It is interesting to note that  $\text{CO}_2$  uptake capacity at 1 bar increases with the increasing atomic number ( $\text{Li} < \text{Na} < \text{K} < \text{Ca}$ ), which is inverse to the trend of BET surface area. The uptake amounts for Zr-tcpb-COOCa is  $33.22\text{ cm}^3\text{ g}^{-1}$  STP ( $1.48\text{ mmol g}^{-1}$ ) at 1 bar. Furthermore, all the cation modified samples demonstrated increases in uptake (increased by 66.5% at 0.05 bar in Zr-tcpb-COOK) within the low-pressure region ( $<0.1$  bar) when compared to the unmodified blank sample Zr-tcpb-COOH (Fig. S8†). This increase in uptake is attributed to the embedded metal sites that have stronger interactions with  $\text{CO}_2$  compared to the free carboxylic acid. Additionally, all samples exhibit negligible uptake of  $\text{N}_2$  at 298 K, indicating their excellent selectivity for  $\text{CO}_2$  over  $\text{N}_2$  ( $\text{CO}_2/\text{N}_2$  IAST selectivity ( $15:85$ ) = 539.5) (Fig. 3d). The high selectivity of  $\text{CO}_2/\text{N}_2$  may be attributed to

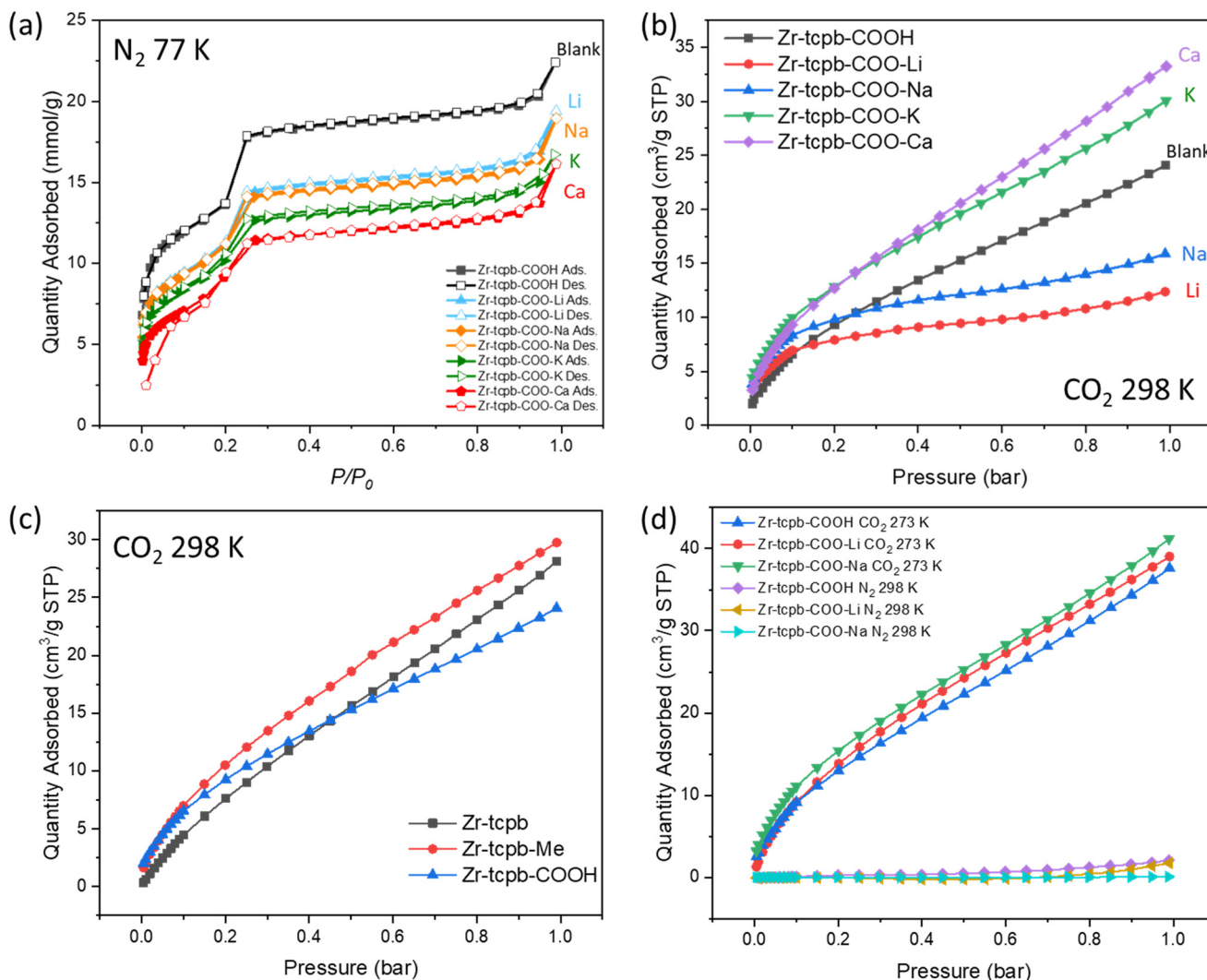


**Fig. 3** The gas adsorption–desorption isotherms of Zr-tcpb-COOM: (a)  $\text{N}_2$  at 77 K and (b)  $\text{CO}_2$  at 298 K; (c) the  $\text{CO}_2$  adsorption isotherms of unmodified Zr-tcpb-X at 298 K; (d) comparisons of adsorption isotherms of  $\text{CO}_2$  and  $\text{N}_2$  at 273 K and 298 K.

the high affinity between the metal sites and  $\text{CO}_2$  while such sites have very little interaction with  $\text{N}_2$ . Our compounds hold the highest  $\text{CO}_2/\text{N}_2$  selectivity (0.15/0.85) among all Zr-based UiO-type MOFs, and the selectivity values are also among the highest when comparing to other stable MOFs such as MIL-101 and JLU-Liu45.<sup>45–47</sup> The dynamic adsorption of water was increased slightly due to the strong interaction of water and metals (Fig. S9†).

#### 3.4 Solid-state NMR analysis

The  $^{13}\text{C}$  CP-MAS NMR spectra of the pristine and post-synthetically modified MOFs were taken (Fig. 4a) and showed changes in the region associated with carboxylic acid groups (170–180 ppm) as a function of metal cation identity added to the material before activation (Fig. 4c). Two overlapping resonances near 171 and 172 ppm are assigned to the four carboxylic acid groups on the linker that coordinate to the zirconium clusters, while carboxylic acid peaks above 174

ppm are assigned as belonging to the non-structural carboxylic acid group on the center benzene ring of the linker, which we will call the sidechain COOH. The ratio of integration of those two peaks in blank sample are 1.79 to 1, which matches with the ratio of different carboxylic acid groups on the building ligand. In the pristine material and in the monovalent cation-modified materials, a single peak is observed for this group, whereas for the  $\text{Ca}^{2+}$ -modified material, three peaks are observed. The sidechain COOH chemical shift increases from the pristine value when the material is post-synthetically modified with cations, suggesting an interaction between the cations and this sidechain COOH. The chemical shift of this group increases in a series from pristine < Na < Li < K < Ca, roughly following a trend down the periodic table with the exception of Na (Fig. 4b and c). To better understand the environment around the metal cations, we performed  $^7\text{Li}$  and  $^{23}\text{Na}$  solid state NMR. The width and symmetry of peaks in NMR spectra of quadrupolar nuclei such as  $^{23}\text{Na}$  or  $^7\text{Li}$  are dependent on

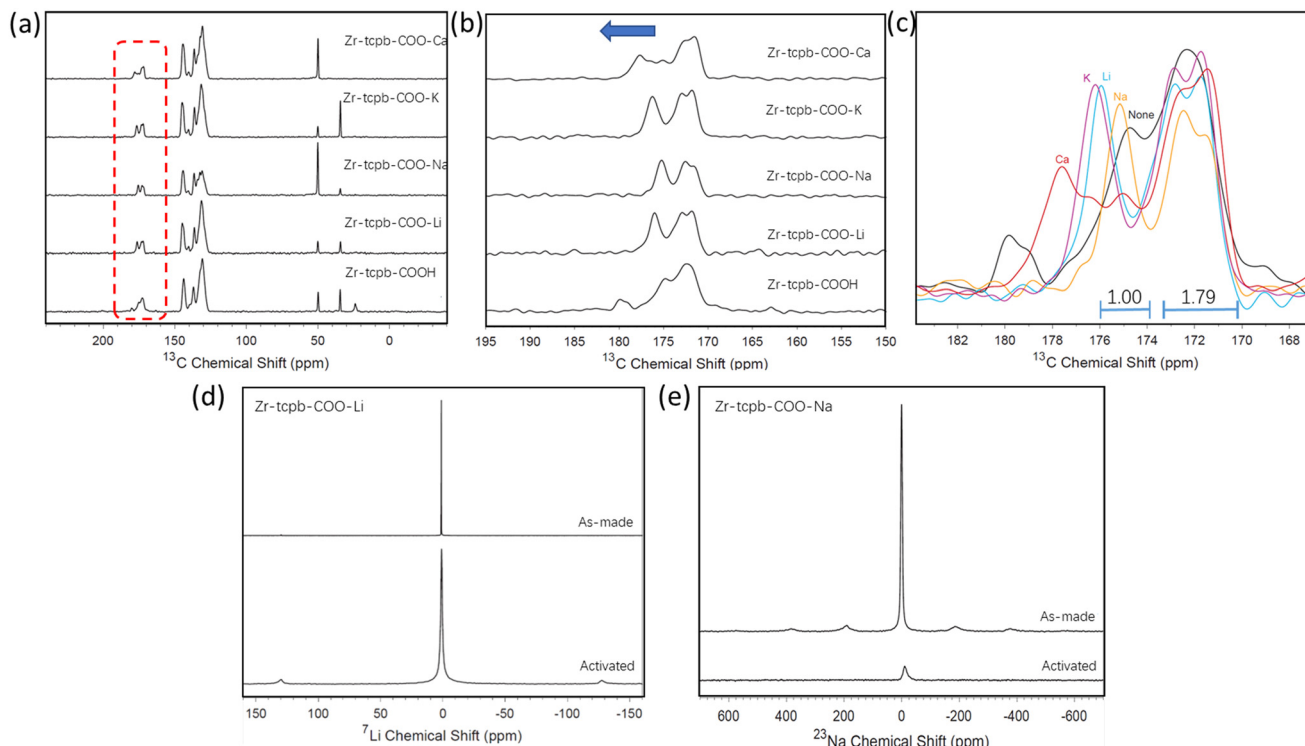


**Fig. 4** Solid-state  $^{13}\text{C}$  CP-MAS NMR spectra of (a) as-made and modified samples; (b) carboxylic acid group region of as-made and modified samples; (c) overlap of carboxylic acid group region.  $^7\text{Li}$  (d) and  $^{23}\text{Na}$  (e) solid state NMR spectra of as-made and modified samples.

the symmetry of the electronic environment around the metal site. In the inactivated as-made materials, narrow resonances are observed in  $^7\text{Li}$  and  $^{23}\text{Na}$  spectra, corresponding to a symmetric environment of water ligands solvating the cations (Fig. 4d and e). After activation, the  $^{23}\text{Na}$  and  $^7\text{Li}$  peaks broaden and shift up field slightly, suggesting a more asymmetric environment around the metal ions (Fig. 4d and e). Peaks attributable to solvent and residual water are still present as observed by  $^{13}\text{C}$  CP-MAS and  $^1\text{H}$  NMR (Fig. S10†), and the  $^{13}\text{C}$  COOH peaks broaden inhomogeneously, suggesting a complex pore environment around the sidechain COOH groups in the activated materials comprised of cations and residual solvent molecules.

### 3.5 Recyclability and chemical stability

The recyclability of the MOF sorbents is a crucial evaluating factor that determines whether the materials have the potential for use in real-world industrial processes. To confirm the recyclability and stability of our compounds, we tested the samples with five consecutive  $\text{CO}_2$  adsorption-desorption cycles. Zr-tcpb-COO-Ca was chosen for the recyclability measurements since it has the highest  $\text{CO}_2$  uptake capacity. After activating the sample under 373 K in nitrogen flow, a  $\text{CO}_2:\text{N}_2$  gas mixture with 95:5 ratio (v:v) was purged inside the sample chamber at 303 K (5%  $\text{N}_2$  as balancing gas). The uptake amount of  $\text{CO}_2$  was monitored by the weight change of the sample. As shown in Fig. 5, the

uptake capacity was found to be  $\sim 1.49 \text{ mmol g}^{-1}$ , matching well with the single component adsorption data. More importantly, the uptake amount remained essentially constant for all five cycles, confirming the high stability and reusability of this sorbent.

Like the other zirconium MOFs with high connectivity, both Zr-tcpb-COOH and Zr-tcpb-COOM also demonstrate high resistance toward harsh conditions. For example, the as-

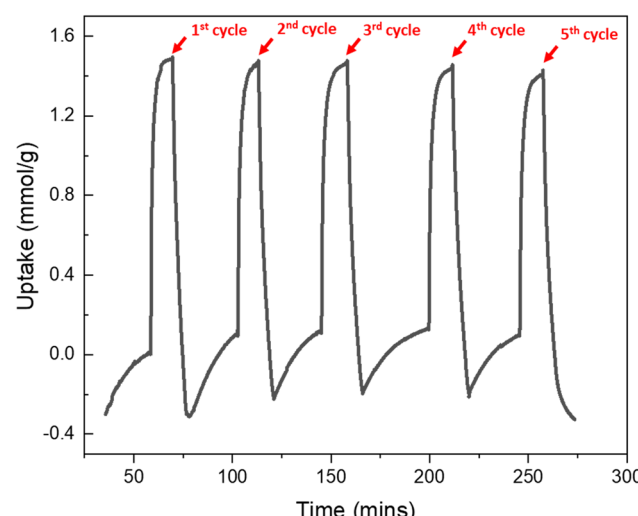


**Fig. 5** The  $\text{CO}_2$  adsorption-desorption recyclability test results for the Zr-tcpb-COO-Ca sample. Five consecutive adsorption cycles were carried out with a gas feeding ratio  $\text{CO}_2:\text{N}_2 = 95:5$  (v:v) at 303 K.

made sample of Zr-tcpb-COOH remained highly crystalline after soaking in concentrated HCl and HNO<sub>3</sub> solution for 3 days and showed good stability in basic solution at low concentrations (up to 0.02 M NaOH). The structure was intact even after 5 months of exposure in open air (Fig. S3a†). The Zr-tcpb-COOM samples also maintained high crystallinity in concentrated HCl and after the recyclability test (Fig. S3b†).

## 4. Conclusion

We have successfully designed and synthesized a series of isoreticular MOFs, Zr-tcpb-COOM, with alkali/alkaline earth metal cations introduced *via* post-synthetic modification. The creation of these metal sites leads to enhancement in carbon dioxide (CO<sub>2</sub>) adsorption capacity, especially at very low CO<sub>2</sub> pressure. The increase in the CO<sub>2</sub> uptake capacity is in trend with the increase of cation's atomic number (Li<sup>+</sup> < Na<sup>+</sup> < K<sup>+</sup> < Ca<sup>2+</sup>). Relatively high adsorption selectivity (CO<sub>2</sub>/N<sub>2</sub> IAST selectivity (15 : 85) = 539.5) for carbon dioxide over nitrogen is achieved at room temperature. Zr-tcpb-COOCa reaches the highest capacity at 298 K and 1 bar among all Zr-tcpb-COOM. Moreover, the Zr-tcpb-COOM series exhibit high chemical stability, thermal stability, and excellent recyclability.

## Author contributions

G. Zhang: methodology, investigation, formal analysis, visualization, writing – original draft. F. Xie: investigation, formal analysis. A. Patel: investigation. T. Popp and A. Nieuwkoop: investigation, formal analysis. E. Morales and K. Tan: investigation, formal analysis. R. Crichton and J. Zhang: investigation, formal analysis. G. Hall: formal analysis. J. Li: conceptualization, supervision, validation, writing – review & editing.

## Conflicts of interest

The authors declare no competing financial interest.

## Acknowledgements

We are grateful for the financial support from the U.S. Department of Energy, Office of Science, Office of Basic Energy Sciences under award No. DE-SC0019902.

## References

- E. S. Sanz-Pérez, C. R. Murdock, S. A. Didas and C. W. Jones, *Chem. Rev.*, 2016, **116**, 11840–11876.
- X. Shi, H. Xiao, H. Azarabadi, J. Song, X. Wu, X. Chen and K. S. Lackner, *Angew. Chem., Int. Ed.*, 2020, **59**, 6984–7006.
- L. Espinal, D. L. Poster, W. Wong-Ng, A. J. Allen and M. L. Green, *Environ. Sci. Technol.*, 2013, **47**, 11960–11975.
- A. Samanta, A. Zhao, G. K. H. Shimizu, P. Sarkar and R. Gupta, *Ind. Eng. Chem. Res.*, 2012, **51**, 1438–1463.
- S. Xiang, Y. He, Z. Zhang, H. Wu, W. Zhou, R. Krishna and B. Chen, *Nat. Commun.*, 2012, **3**, 954.
- H. Lyu, O. I.-F. Chen, N. Hanikel, M. I. Hossain, R. W. Flaig, X. Pei, A. Amin, M. D. Doherty, R. K. Impastato, T. G. Glover, D. R. Moore and O. M. Yaghi, *J. Am. Chem. Soc.*, 2022, **144**, 2387–2396.
- H. Mao, J. Tang, G. S. Day, Y. Peng, H. Wang, X. Xiao, Y. Yang, Y. Jiang, S. Chen, D. M. Halat, A. Lund, X. Lv, W. Zhang, C. Yang, Z. Lin, H.-C. Zhou, A. Pines, Y. Cui and J. A. Reimer, *Sci. Adv.*, 2022, **8**, eab06849.
- J. Wang, L. Huang, R. Yang, Z. Zhang, J. Wu, Y. Gao, Q. Wang, D. O'Hare and Z. Zhong, *Energy Environ. Sci.*, 2014, **7**, 3478–3518.
- M. Ding, R. W. Flaig, H.-L. Jiang and O. M. Yaghi, *Chem. Soc. Rev.*, 2019, **48**, 2783–2828.
- Z. Hu, Y. Wang, B. B. Shah and D. Zhao, *Adv. Sustainable Syst.*, 2019, **3**, 1800080.
- J.-B. Lin, T. T. T. Nguyen, R. Vaidhyanathan, J. Burner, J. M. Taylor, H. Durekova, F. Akhtar, R. K. Mah, O. Ghaffari-Nik, S. Marx, N. Fylstra, S. S. Iremonger, K. W. Dawson, P. Sarkar, P. Hovington, A. Rajendran, T. K. Woo and G. K. H. Shimizu, *Science*, 2021, **374**, 1464–1469.
- H. Wu, R. S. Reali, D. A. Smith, M. C. Trachtenberg and J. Li, *Chemistry*, 2010, **16**, 13951–13954.
- J. Cure, E. Mattson, K. Cocq, H. Assi, S. Jensen, K. Tan, M. Catalano, S. Yuan, H. Wang, L. Feng, P. Zhang, S. Kwon, J.-F. Veyan, Y. Cabrera, G. Zhang, J. Li, M. Kim, H.-C. Zhou, Y. J. Chabal and T. Thonhauser, *J. Mater. Chem. A*, 2019, **7**, 17536–17546.
- M. J. Lashaki, S. Khiavi and A. Sayari, *Chem. Soc. Rev.*, 2019, **48**, 3320–3405.
- J. H. Choe, H. Kim, M. Kang, H. Yun, S. Y. Kim, S. M. Lee and C. S. Hong, *J. Am. Chem. Soc.*, 2022, **144**, 10309–10319.
- B. Dinakar, A. C. Forse, H. Z. H. Jiang, Z. Zhu, J.-H. Lee, E. J. Kim, S. T. Parker, C. J. Pollak, R. L. Siegelman, P. J. Milner, J. A. Reimer and J. R. Long, *J. Am. Chem. Soc.*, 2021, **143**, 15258–15270.
- T. M. McDonald, J. A. Mason, X. Kong, E. D. Bloch, D. Gygi, A. Dani, V. Crocellà, F. Giordanino, S. O. Odoh, W. S. Drisdell, B. Vlaislavljevich, A. L. Dzubak, R. Poloni, S. K. Schnell, N. Planas, K. Lee, T. Pascal, L. F. Wan, D. Prendergast, J. B. Neaton, B. Smit, J. B. Kortright, L. Gagliardi, S. Bordiga, J. A. Reimer and J. R. Long, *Nature*, 2015, **519**, 303–308.
- R. W. Flaig, T. M. O. Popp, A. M. Fracaroli, E. A. Kapustin, M. J. Kalmutzki, R. M. Altamimi, F. Fathieh, J. A. Reimer and O. M. Yaghi, *J. Am. Chem. Soc.*, 2017, **139**, 12125–12128.
- C. E. Bien, K. K. Chen, S.-C. Chien, B. R. Reiner, L.-C. Lin, C. R. Wade and W. S. W. Ho, *J. Am. Chem. Soc.*, 2018, **140**, 12662–12666.
- C. E. Bien, Q. Liu and C. R. Wade, *Chem. Mater.*, 2020, **32**, 489–497.
- Z. Cai, C. E. Bien, Q. Liu and C. R. Wade, *Chem. Mater.*, 2020, **32**, 4257–4264.
- H. Wang, J. Peng and J. Li, *Chem. Rec.*, 2016, **16**, 1298–1310.
- A. Torrisi, R. G. Bell and C. Mellot-Draznieks, *Cryst. Growth Des.*, 2010, **10**, 2839–2841.

24 H. Huang, W. Zhang, F. Yang, B. Wang, Q. Yang, Y. Xie, C. Zhong and J.-R. Li, *Chem. Eng. J.*, 2016, **289**, 247–253.

25 N. Li, Z. Chang, H. Huang, R. Feng, W. W. He, M. Zhong, D. G. Madden, M. J. Zaworotko and X. H. Bu, *Small*, 2019, **15**, e1900426.

26 A. L. Dzubak, L.-C. Lin, J. Kim, J. A. Swisher, R. Poloni, S. N. Maximoff, B. Smit and L. Gagliardi, *Nat. Chem.*, 2012, **4**, 810–816.

27 X. Kong, E. Scott, W. Ding, J. A. Mason, J. R. Long and J. A. Reimer, *J. Am. Chem. Soc.*, 2012, **134**, 14341–14344.

28 B. Liu, S. Yao, X. Liu, X. Li, R. Krishna, G. Li, Q. Huo and Y. Liu, *ACS Appl. Mater. Interfaces*, 2017, **9**, 32820–32828.

29 M. Jia, J. Li, J. Gu, L. Zhang and Y. Liu, *Mater. Chem. Front.*, 2021, **5**, 1398–1404.

30 H. A. Evans, D. Mullangi, Z. Deng, Y. Wang, S. B. Peh, F. Wei, J. Wang, C. M. Brown, D. Zhao, P. Canepa and A. K. Cheetham, *Sci. Adv.*, 2022, **8**, eade1473.

31 J. S. Choi, J. Bae, E. J. Lee and N. C. Jeong, *Inorg. Chem.*, 2018, **57**, 5225–5231.

32 A. Ö. Yazaydin, A. I. Benin, S. A. Faheem, P. Jakubczak, J. J. Low, R. R. Willis and R. Q. Snurr, *Chem. Mater.*, 2009, **21**, 1425–1430.

33 E. D. Bloch, D. Britt, C. Lee, C. J. Doonan, F. J. Uribe-Romo, H. Furukawa, J. R. Long and O. M. Yaghi, *J. Am. Chem. Soc.*, 2010, **132**, 14382–14384.

34 S. Shang, C. Yang, M. Sun, Z. Tao, A. Hanif, Q. Gu and J. Shang, *Sep. Purif. Technol.*, 2022, **301**, 122058.

35 S. J. Datta, C. Khumnoon, Z. H. Lee, W. K. Moon, S. Docao, T. H. Nguyen, I. C. Hwang, D. Moon, P. Oleynikov, O. Terasaki and K. B. Yoon, *Science*, 2015, **350**, 302–306.

36 M. Lammert, H. Reinsch, C. A. Murray, M. T. Wharmby, H. Terraschke and N. Stock, *Dalton Trans.*, 2016, **45**, 18822–18826.

37 Z. Chen, S. L. Hanna, L. R. Redfern, D. Alezi, T. Islamoglu and O. K. Farha, *Coord. Chem. Rev.*, 2019, **386**, 32–49.

38 G. Zhang, K. Tan, S. Xian, K. Xing, H. Sun, G. Hall, L. Li and J. Li, *Inorg. Chem.*, 2021, **60**, 11730–11738.

39 K. I. Hadjiivanov, D. A. Panayotov, M. Y. Mihaylov, E. Z. Ivanova, K. K. Chakarova, S. M. Andonova and N. L. Drenchev, *Chem. Rev.*, 2021, **121**, 1286–1424.

40 E. Velasco, Y. Osumi, S. J. Teat, S. Jensen, K. Tan, T. Thonhauser and J. Li, *Chemistry*, 2021, **3**, 327–337.

41 K. Tan, N. Nijem, P. Canepa, Q. Gong, J. Li, T. Thonhauser and Y. J. Chabal, *Chem. Mater.*, 2012, **24**, 3153–3167.

42 H.-Q. Yin, K. Tan, S. Jensen, S. J. Teat, S. Ullah, X. Hei, E. Velasco, K. Oyekan, N. Meyer, X.-Y. Wang, T. Thonhauser, X.-B. Yin and J. Li, *Chem. Sci.*, 2021, **12**, 14189–14197.

43 K. Tan, S. Zuluaga, Q. Gong, P. Canepa, H. Wang, J. Li, Y. J. Chabal and T. Thonhauser, *Chem. Mater.*, 2014, **26**, 6886–6895.

44 N. Planas, J. E. Mondloch, S. Tussupbayev, J. Borycz, L. Gagliardi, J. T. Hupp, O. K. Farha and C. J. Cramer, *J. Phys. Chem. Lett.*, 2014, **5**, 3716–3723.

45 X. Sun, X. Li, S. Yao, R. Krishna, J. Gu, G. Li and Y. Liu, *J. Mater. Chem. A*, 2020, **8**, 17106–17112.

46 W. Zhang, H. Huang, C. Zhong and D. Liu, *Phys. Chem. Chem. Phys.*, 2012, **14**, 2317–2325.

47 K. Munusamy, G. Sethia, D. V. Patil, P. B. S. Rallapalli, R. S. Soman and H. C. Bajaj, *Chem. Eng. J.*, 2012, **195–196**, 359–368.